

An Online Generalized Multiscale finite element method for heat and mass transfer problem with artificial ground freezing

Denis Spiridonov ^{*} Sergei Stepanov [†] Vasiliy Vasil'ev [‡]

May 31, 2022

Abstract

The Online Generalized Multiscale Finite Element Method (Online GMsFEM) is presented in this study for heat and mass transfer problem in heterogeneous media with artificial ground freezing process. The mathematical model is based on the classical Stefan model, which depicts heat transfer with a phase change and includes filtration in a porous media. The model is described by a set of temperature and pressure equations. We employ a finite element method with the fictitious domain method to solve the problem on a fine grid. We apply a model reduction approach based on Online GMsFEM to derive a solution on the coarse grid. We can use the online version of GMsFEM to take less offline multiscale basis functions. We use decoupled offline basis functions built with snapshot space and based on spectral problems in our method. This is the standard approach of basis construction. We calculate additional basis functions in the offline stage to account for artificial ground freezing pipes. We use online multiscale basis functions to get a more precise approximation of phase change. We create an online basis that reduces error using local residual values. The accuracy of standard GMsFEM is greatly improved by using an online approach. Numerical results in a two-dimensional domain with layered heterogeneity are presented. To test the method's accuracy, we show results from a variety of offline and online basis functions. The results suggest that Online GMsFEM can deliver high-accuracy solutions with minimal processing resources.

Keywords: Heat and mass transfer problem, Stefan problem, phase change, artificial ground freezing, multiscale finite element method, Online Generalized multiscale finite element method, multiscale model reduction

1 Introduction

In this research, we investigate at a heat and mass transfer process with artificial ground freezing. Almost every aspect of building and mining uses artificially frozen filter soils [1–5]. For example, such technology is

^{*}Laboratory of Computational Technologies for Modeling Multiphysical and Multiscale Permafrost Processes, North-Eastern Federal University, 677000 Yakutsk, Republic of Sakha (Yakutia), Russia. Email: d.stalnov@mail.ru.

[†]Laboratory of Computational Technologies for Modeling Multiphysical and Multiscale Permafrost Processes, North-Eastern Federal University, 677000 Yakutsk, Republic of Sakha (Yakutia), Russia Email: cepe2a@inbox.ru.

[‡]Department of Computational technologies, North-Eastern Federal University, 677000 Yakutsk, Republic of Sakha (Yakutia), Russia Email: vasvasil@mail.ru.

commonly utilized in mine sinking, tunneling, subway construction, and building construction, etc. Artificial freezing with cooling equipment is employed near piles in the construction of buildings on permafrost soils to assure stability by generating big chunks of frozen earth surrounding the pile, which will preserve the soil from defrosting throughout the summer [6–8]. This practice has been demonstrated to strengthen building foundations in the Far North.

The authors describe mathematical models of heat and mass transfer processes in frozen and thawed soils, as well as artificial freezing of filter soils in the works [9,10]. A set of heat and mass transfer equations with a dynamic phase transition boundary is solved, which comprises a parabolic equation for temperature and an elliptic equation for pressure. We employ a finite element method to approximate problem on the fine grid. [11,12]. We apply the through counting approach to model temperature phase change [13,14] and the fictional domain method to model pressure phase change [15,16].

These processes are generally modeled in very huge domains where the construction body is located. It is important to construct a highly fine computational grid in order to precisely describe the process at each point in a large region. This method demands high computational prices and high-end computing hardware, such as a supercomputer. As a way out of the situation, You can utilize homogenization methods [8,17–19] just design coarser grids to get out of the problem, but the accuracy of the solution will suffer. We propose a model reduction technique based on multiscale finite element method [20].

Multiscale finite element method(MsFEM) is particularly suited for modeling problems in highly heterogeneous regions [21,22]. Multiscale methods come in many forms, such as multiscale finite volume method (MsFVM) [23–26] which uses the finite volume method to generate the basis functions [27,28]. Another MsFEM modification is the generalized finite element method(GMsFEM) [29–31] which builds several bases in each local domain by solving local spectral problems. In the constraint energy minimizing generalized multiscale finite element method(CEM-GMsFEM), the basis building can be provided in an oversampled domain [32–34]. A multiscale method that satisfies the properties of mass conservation is called mixed multiscale finite element method (Mixed MsFEM) [35–37]. An online generalized multiscale finite element method (Online GMsFEM) [38–41] is particularly suited for nonlinear problems because it executes the procedure of enriching a multiscale space during the online stage of the method. A special type of multiscale basis functions based on constrained energy minimization problems are developed in [42–45] and well-known as nonlocal multicontinuum method(NLMC).

We previously created a GMsFEM algorithm with an additional basis function for artificial ground freezing [46]. We expand our technique and employ multiscale online basis functions to predict phase change in the heat and mass transfer problem with artificial ground freezing in this study. We perform a model reduction procedure which includes offline and online stage. We create offline basis functions using local spectral problems in the offline stage. To better forecast processes in mediums with high contrast, we use snapshot space in basis computation. The considered medium features layered heterogeneity with a large value jump between two layers. In the computational domain, our problem involves frozen pipes. We employ offline additional basis functions to account the effect of frozen pipes in order to make an accurate simulation. In the online stage, we construct an online multiscale basis functions. They assist in the accurate approximation of a shifting phase change boundary. Local residuals are used to compute online

basis functions. Using online bases allows us to take smaller amount of offline basis functions with better accuracy.

The numerical results are shown in a two-dimensional heterogeneous domain. We consider a two type of boundary condition for pressure. In the first example we set flow from right to left and in the second example we set flow from top to bottom. We complete the validation process by showing the results for a variety of offline and online basis functions.

The paper organized as follows. In Section 2, we present a mathematical model for heat and mass transfer problem with numerical algorithm for phase change boundary. In Section 3, we present an approximation on the fine grid using finite element method. Next, in Section 4, we describe an algorithm of online generalized multiscale finite element method. Numerical results for two test cases are presented in Section 5.

2 Problem formulation

We consider the heat and mass transfer model with artificial ground freezing. Freezing pipes within the soils enable artificial ground freezing process. We use the classical Stefan model to simulate heat transfer processes with phase change [47, 48]. In this approximation, we assume that the phase change occurs at a given phase change temperature T^* . Let $\Omega^+(t)$ is the domain of the liquid phase where the temperature exceeds the phase change temperature:

$$\Omega^+(t) = \{x \mid x \in \Omega, T(x, t) > T^*,$$

and $\Omega^-(t)$ is the domain of frozen phase:

$$\Omega^-(t) = \{x \mid x \in \Omega, T(x, t) < T^*,$$

We denote by ρ^+, c^+ and ρ^-, c^- the density and specific heat capacity of the liquid and frozen zones, respectively. We define the indicator function as piecewise defined function

$$\phi = \phi(T) = \begin{cases} 0, & T < T^*, \\ 1, & T > T^*. \end{cases}$$

For the coefficients of heat capacity and thermal conductivity, we have

$$\alpha(\phi) = \rho^- c^- + \phi(\rho^+ c^+ - \rho^- c^-), \quad k(\phi) = k^- + \phi(k^+ - k^-).$$

Thermal processes, which are accompanied by phase change, absorption and release of latent heat of fusion, are described by the equation

$$\left(\alpha(\phi) + \rho^+ L \frac{\partial \phi}{\partial t} \right) \left(\frac{\partial T}{\partial t} + u \nabla T \right) - \nabla \cdot (k(\phi) \nabla T) = Q. \quad (1)$$

Here L is the specific heat of the phase change, u is the filtration speed in the soil.

We have heat capacity coefficients because we are considering heat transfer in a porous material:

$$c^- \rho^- = (1 - m) c_{sc} \rho_{sc} + m c_l \rho_l, \quad c^+ \rho^+ = (1 - m) c_{sc} \rho_{sc} + m c_w \rho_w,$$

here m is the porosity and the subscripts sc , w , and l denote the skeleton of porous medium, water and ice, respectively. We use comparable terms for heat conductivity coefficients in the solid and frozen zones:

$$\lambda^- = (1 - m)\lambda_{sc} + m\lambda_l, \quad \lambda^+ = (1 - m)\lambda_{sc} + m\lambda_w.$$

To take into account the filtration in the soil, we write the continuity equation for a completely saturated porous medium

$$\frac{\partial}{\partial t}(\rho_w m) + \nabla \cdot (\rho_w u) = 0. \quad (2)$$

We use Darcy's law to express the relationship between the filtration rate u and the pressure gradient:

$$u = -\frac{k}{\mu}(\nabla p + \rho_w g), \quad (3)$$

where k is the absolute permeability tensor of the porous medium, μ is the fluid viscosity, g is the free fall acceleration and ρ_w is the density of water.

Substituting (3) into (2) and neglecting compressibility for simplicity, we obtain equations for determining reservoir pressure

$$-\nabla \cdot (\lambda \nabla p) = F, \quad x \in \Omega^+, \quad (4)$$

where $\lambda = \rho_w k / \mu$.

The system of equations (1), (4) is the base for modeling the processes of thermal stabilization of filter soils. In our problem the main difficulties of numerical simulation are generated by the phase change, we need to solve the filtration problem with a free (unknown) boundary. We use computational algorithms for through counting, which were used by many authors in solving similar problems of heat and mass transfer with phase transformations [49–51].

In our implementation we assume that the phase change occurs not when $T^* = T$, but in some small interval near the temperature of phase change $[T^* - \delta, T^* + \delta]$. Instead of the indicator function ϕ , we take its piecewise linear approximation of the following form:

$$\phi_\delta(T) = \begin{cases} 0, & T \leq T^* - \Delta, \\ \frac{T - T^* + \Delta}{2\Delta}, & T^* - \Delta < T < T^* + \Delta, \\ 1, & T \geq T^* + \Delta. \end{cases}$$

Then, we have

$$\frac{d\phi_\Delta}{dT} = \begin{cases} 0, & T < T^* - \Delta, \\ \frac{1}{2\Delta}, & T^* - \Delta < T < T^* + \Delta, \\ 0, & T > T^* + \Delta. \end{cases}$$

Thus, instead of (1) in the computational domain Ω , we solve the following equation for temperature:

$$\left(\alpha(\phi_\Delta) + \rho^+ L \frac{d\phi_\Delta}{dT} \right) \left(\frac{\partial T}{\partial t} + u \nabla T \right) - \nabla \cdot (k(\phi_\Delta) \nabla T) = Q \quad (5)$$

This non-linear parabolic equation is supplemented with appropriate initial and boundary conditions.

Since our problem (4)-(5) has a moving phase transition boundary, we are faced with the problem of constructing a numerical algorithm for calculating the pressure. For the numerical solution of such a problem without rebuilding the computational grid, we use the method of fictitious domain, which is based on the transition to solving the problem in a wider domain. An approximate solution, depending on the continuation parameter ε , we will solve in the entire computational domain Ω . When using a variant of the method of fictitious regions with continuation by leading coefficients, the solution is determined from the equation

$$\nabla \cdot (\lambda_\varepsilon \nabla p) = F, \quad x \in \Omega. \quad (6)$$

Here, the discontinuous coefficient $\lambda_\varepsilon(x)$ is determined by the expression

$$\lambda_\varepsilon(x) = \begin{cases} \lambda, & x \in \Omega^+, \\ \lambda\varepsilon, & x \in \Omega^- \end{cases} \quad (7)$$

with very small ε . With this choice of coefficients, equation (6) simulates filtration in the region Ω^- with a very small coefficient $\lambda_\varepsilon(x) \rightarrow 0$ with the parameter $\varepsilon \rightarrow 0$.

We supplement our system (5),(6) with appropriate initial and boundary conditions. For temperature, we apply the initial condition:

$$T = T_0(x), \quad x \in \Omega. \quad (8)$$

As the boundary condition for the temperature, we take the zero Neumann boundary condition over the entire boundary of the computational domain:

$$-k \frac{\partial T}{\partial n} = 0, \quad x \in \partial\Omega. \quad (9)$$

In our problem we have an artificial ground freezing process. To simulate it, we set the following boundary condition on the pipes:

$$T = T_p, \quad x \in \Gamma_p \quad (10)$$

where Γ_p is the boundary of artificial ground freezing pipes.

For the pressure, we set boundary conditions on the boundary of the entire computational domain $\partial\Omega = \Gamma_N \cup \Gamma_D$:

$$-\lambda_\varepsilon \frac{\partial p}{\partial n} = 0, \quad x \in \Gamma_N, \quad p = q_D, \quad x \in \Gamma_D, \quad (11)$$

When using the computational algorithm for through counting, it is necessary to pay special attention to setting the parameters Δ and ε . These parameters indicate the width of the phase transition, they determine the accuracy of the phase change boundary for solving on a fine grid. Δ and ε depend on the dimension of the grid, for an accurate approximation, a sufficient number of grid elements within the phase transition is required. In the paper, we chose these parameters based on the works [52, 53], where the authors studied the influence of hyperparameters on the solution of the problem with a phase change.

3 Fine grid approximation

Let us discretize in space using the finite element method of the initial-boundary value problem (5),(6), (8)-(11) for the resulting basic system of equations, which is used to simulate artificial freezing processes. To reformulate the original system of temperature and pressure equations, we multiply equation (5) by the test functions v , and equation (6) by the test function w . We integrate our system using Green's formula and boundary conditions (6), (7) and obtain the following formulation:

$$\begin{aligned} \int_{\Omega} \left(\alpha(\phi_{\Delta}) + \rho^+ L \frac{d\phi_{\Delta}}{dT} \right) \left(\frac{\partial T}{\partial t} + u \nabla T \right) v dx + \int_{\Omega} (k(\phi_{\Delta}) \nabla T, \nabla v) dx &= \int_{\Omega} Q v dx, \quad \forall v \in H_0^1(\Omega), \\ \int_{\Omega} (\lambda_{\varepsilon} \nabla p, \nabla w) dx &= \int_{\Omega} F w dx, \quad \forall w \in H_0^1(\Omega). \end{aligned} \quad (12)$$

Here $H^1(\Omega)$ is Sobolev space that consist of functions q such that q^2 and $|\nabla q|^2$ have a finite integral in Ω and $H_0^1(\Omega) = \{q \in H^1(\Omega) : q(x) = 0, x \in \Gamma_P\}$.

To approximate the equation for temperature in time, we use the standard implicit scheme. The simplest linearization is used when specifying the coefficients from the previous time layer. Let $t_{max} = n\tau$, $n = 1, 2, \dots, N_t$ and τ be the time step. We denote the solution at time t_n by T^n , p^n . According to (12) we can derive a variational formulation:

$$\begin{aligned} \int_{\Omega} \left(\alpha(\phi_{\Delta}^n) + \rho^+ L \frac{d\phi_{\Delta}}{dT}(T^n) \right) \left(\frac{T^{n+1} - T^n}{\tau} + (\lambda_{\varepsilon}^n \nabla p^n \nabla T^n) \right) v dx + \\ + \int_{\Omega} (k(\phi_{\Delta}^n) \nabla T^{n+1}, \nabla v) dx &= \int_{\Omega} Q v dx, \quad \forall v \in H_0^1(\Omega), \\ \int_{\Omega} (\lambda_{\varepsilon}^n \nabla p^{n+1}, \nabla w) dx &= \int_{\Omega} F w dx, \quad \forall w \in H_0^1(\Omega) \end{aligned} \quad (13)$$

Let write approximation in the matrix form:

$$\begin{aligned} S_T^n \frac{T^{n+1} - T^n}{\tau} + A_T^n T^{n+1} &= G_T, \\ A_p^n p^{n+1} &= G_p. \end{aligned} \quad (14)$$

Approximation in space (13) is associated with the choice of the corresponding finite element spaces for temperature and pressure and is carried out in the standard way. For both temperature and pressure, we use Lagrangian finite elements of the first order on a triangular mesh.

4 Coarse grid approximation

To make approximation on the coarse grid, we apply an Online Generalized Multiscale Finite Element method. A coarse grid \mathcal{TH} is denoted by

$$\mathcal{T}_H = \bigcup_j K_j,$$

here K_j is the cell of coarse grid. Following that, we create a local coarse neighborhood domain ω_i it is produced by merging all coarse cells around one coarse grid vertex:

$$\omega_i = \bigcup_j K_j \in \mathcal{T} : x_i \in K_j,$$

where $i = \overline{1, N_c}$ and N_c – the number of coarse grid vertices.

We can identify two stages in GMSFEM: online and offline:

Offline stage:

1. Creating local coarse neighborhood domains ω_i from the coarse grid;
2. In each local domain ω_i we construct an offline multiscale basis functions;
3. Construction an additional basis function for temperature T in each local domain ω_i that contains ground freezing pipes;
4. Assembling a projection matrix R of the multiscale space. This matrix consist of offline basis functions.

Online stage:

1. Assembling a system of equations on fine grid and projecting it on the multiscale space by R matrix;
2. Solving a system of equations on the coarse grid by the resulting approximation on a coarse grid;
3. Constructing an online multiscale basis functions on certain time layers;
4. Resolving system on the coarse grid using new matrix R^{on} with online bases.

We should note, that we perform steps 3 and 4 only on certain time steps, otherwise we skip this steps. We add online bases not on every time layer, for example, we can do it on every 5-th or 10-th time layers. Following that, we go over the GMSFEM algorithm in further detail.

4.1 Offline stage

Snapshot space.

First, to build an offline multiscale basis functions, we need to define a snapshot space for temperature V_T^{snap} and for pressure V_p^{snap} . Therefore, we have to build projection matrices for these spaces. We solve the following problems in each local domain ω_i to identify the matrix's members:

- For temperature:

$$\begin{cases} -\nabla \cdot (k^+ \nabla \varphi_{T,j}^i) = 0, & x \in \omega_i, \\ \varphi_{T,j}^i = \delta_j, & x \in \partial\omega_i. \end{cases} \quad (15)$$

- For pressure:

$$\begin{cases} -\nabla \cdot (\lambda \nabla \varphi_{p,j}^i) = 0, & x \in \omega_i, \\ \varphi_{p,j}^i = \delta_j, & x \in \partial\omega_i. \end{cases} \quad (16)$$

where δ_j is the discrete delta function which equal 1 at the j -th fine grid node $x = x_j$ and zero elsewhere ($j = 1, \dots, J_i$, J_i is a number of fine grid vertices on boundary $\partial\omega_i$). And $\partial\omega_i$ is the outer boundary of local domain ω_i .

The purpose of creating a snapshot space must be discussed. Almost all applied problems are modeled in domains with high coefficient contrast. Such domains may contain fractures or channels. We will compute our problem in domain with high coefficient contrast. We also need to employ a snapshot space to account all important properties of the solution and produce a good approximation. The snapshot vectors can describe most important characteristics of computational domain and help to construct more accurate projection to multiscale space.

Now we can define a snapshot spaces and projection matrices for temperature and pressure:

$$\begin{aligned} V_T^{snap,i} &= \text{span}\{\varphi_{T,1}^i, \dots, \varphi_{T,J_i}^i\}, & R_T^{snap,i} &= (\varphi_{T,1}^i, \dots, \varphi_{T,J_i}^i)^T, \\ V_p^{snap,i} &= \text{span}\{\varphi_{p,1}^i, \dots, \varphi_{p,J_i}^i\}, & R_p^{snap,i} &= (\varphi_{p,1}^i, \dots, \varphi_{p,J_i}^i)^T. \end{aligned} \quad (17)$$

Spectral problem.

The next step of offline multiscale basis construction is computing spectral problems in each local domain ω_i . We should mention that we build a decoupled multiscale basis functions. To obtain a set of basis functions, we solve next eigenvalue problems:

- For temperature:

$$\tilde{A}_T^i \tilde{\Psi}_{T,j}^i = \tilde{\lambda} \tilde{S}_T^i \tilde{\Psi}_{T,j}^i, \quad (18)$$

with

$$\tilde{A}_T^i = R_T^{snap,i} A_T^i (R_T^{snap,i})^T, \quad \tilde{S}_T^i = R_T^{snap,i} S_T^i (R_T^{snap,i})^T,$$

where

$$\begin{aligned} A_T^i &= a_{ln}, & a_{ln} &= \int_{\omega_i} (k^+ \nabla \psi_{m,l}, \nabla \psi_{m,n}) dx \\ S_T^i &= a_{ln}, & a_{ln} &= \int_{\omega_i} (k^+ \psi_{m,l}, \psi_{m,n}) dx \end{aligned}$$

- For pressure

$$\tilde{A}_p^i \tilde{\Psi}_{p,j}^i = \tilde{\lambda} \tilde{S}_p^i \tilde{\Psi}_{p,j}^i, \quad (19)$$

with

$$\tilde{A}_p^i = R_p^{snap,i} A_p^i (R_p^{snap,i})^T, \quad \tilde{S}_p^i = R_p^{snap,i} S_p^i (R_p^{snap,i})^T,$$

where

$$\begin{aligned} A_p^i &= a_{ln}, & a_{ln} &= \int_{\omega_i} (\lambda \nabla \psi_{m,l}, \nabla \psi_{m,n}) dx \\ S_p^i &= a_{ln}, & a_{ln} &= \int_{\omega_i} (\lambda \psi_{m,l}, \psi_{m,n}) dx \end{aligned}$$

Then we obtain solutions of spectral problems on ω_i space $\Psi_{T,j}^i = R_T^{snap,i} \tilde{\Psi}_{T,j}^i$, $\Psi_{p,j}^i = R_p^{snap,i} \tilde{\Psi}_{p,j}^i$. We generate offline multiscale basis functions using the initial M_i eigenvectors that correspond to the smallest M_i eigenvalues.

Multiscale space.

To get offline bases, we utilize the following formula:

$$\psi_{T,j}^i = \Psi_{T,j}^i \chi^i, \quad \psi_{p,j}^i = \Psi_{p,j}^i \chi^i. \quad (20)$$

Where χ^i is the linear partition of unity function that equals to standard coarse grid nodal basis function and $j = 1, \dots, M_i$. The example of first 4 offline multiscale basis functions in one local domain ω_i is presented in Figure 1.

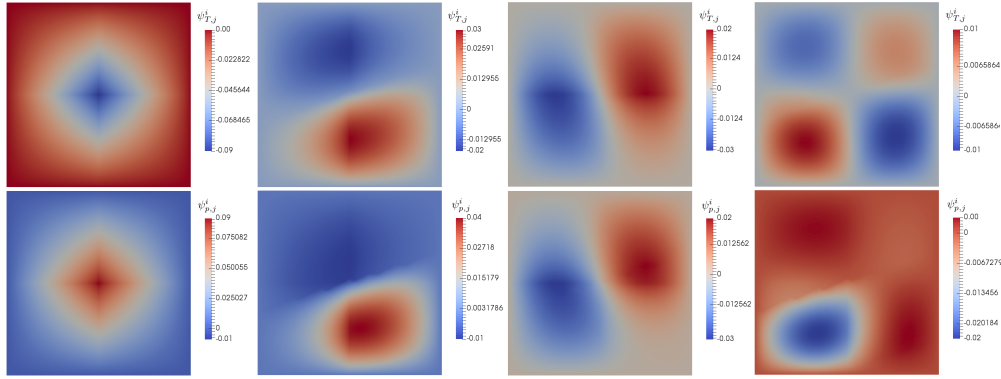


Figure 1: The example of 4 offline multiscale basis functions in ω_i . First row: bases for temperature. Second row: bases for pressure.

After that, we'll be able to create multiscale spaces

$$V_{ms}^T = \text{span}\{\psi_{T,1}^1, \dots, \psi_{T,N_c}^1, \dots, \psi_{T,1}^{N_c}, \dots, \psi_{T,N_c}^{N_c}\},$$

$$V_{ms}^p = \text{span}\{\psi_{p,1}^1, \dots, \psi_{p,N_c}^1, \dots, \psi_{p,1}^{N_c}, \dots, \psi_{p,N_c}^{N_c}\},$$

and projection matrices

$$R_T = (\psi_{T,1}^1, \dots, \psi_{T,N_c}^1, \dots, \psi_{T,1}^{N_c}, \dots, \psi_{T,N_c}^{N_c})^T,$$

$$R_p = (\psi_{p,1}^1, \dots, \psi_{p,N_c}^1, \dots, \psi_{p,1}^{N_c}, \dots, \psi_{p,N_c}^{N_c})^T.$$

Additional offline multiscale basis function.

In our problem, we have freezing pipes in modeling of temperature field. We must consider the impact of boundary condition Γ_P . To calculate additional basis functions for temperature, we solve the next local problem in each local domain that includes freezing pipes

$$\begin{cases} -\nabla \cdot (k^+ \nabla \Psi_{add}^i) = 0, & x \in \omega_i, \\ \Psi_{add}^i = 0, & x \in \partial\omega_i, \\ \Psi_{add}^i = T_p, & x \in \Gamma_P. \end{cases} \quad (21)$$

Then we multiply the solution of local problem (21) on partition of unity function to obtain an additional basis function $\psi_{add}^i = \Psi_{add}^i \chi^i$. It should be noted, that the calculation of additional bases does not depend on the location of the freezing pipes, they can be both inside the coarse block and coincide with the coarse edges. One can see it in the solution of problem (21) in Figure 2.

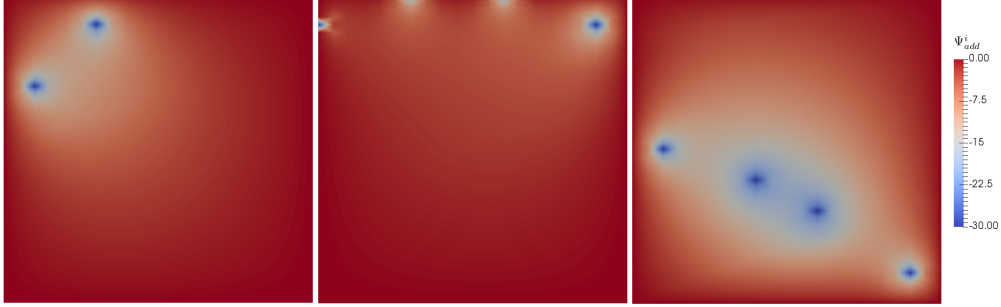


Figure 2: The solution of local problem 21 in three local domains ω_i .

As a result, we get the following multiscale space and projection matrix for temperature:

$$V_{ms}^T = \text{span}\{\psi_{T,1}^1, \dots, \psi_{T,N_c}^1, \dots, \psi_{T,1}^{N_c}, \dots, \psi_{T,N_c}^{N_c}, \psi_{add}^1, \dots, \psi_{add}^{N_p}\},$$

$$R_T = (\psi_{T,1}^1, \dots, \psi_{T,N_c}^1, \dots, \psi_{T,1}^{N_c}, \dots, \psi_{T,N_c}^{N_c}, \psi_{add}^1, \dots, \psi_{add}^{N_p})^T,$$

where N_p is the number of ω_i with ground freezing pipes.

4.2 Online stage

One can see that in offline basis construction we didn't take into account the phase change. We use thermal conductivity k and porous medium permeability λ from liquid zone. We can't take into account the phase change by offline bases, because it changes by time. We can neglect the phase transition, as we did earlier in [54], but in this paper we will take into account the phase change by online multiscale basis functions. The Online GmsFEM is well suited for solving non-linear problems. This method can significantly reduce the number of offline basis functions with good improvement in accuracy. It is better to add 1 or 2 online basis in each ω_i then computing a large number of offline bases. But this process has a big computational cost, because of this we compute online bases only in certain time layer, for example, in each 5-th or 10-th time layer. We construct an online multiscale basis function based on local residuals that provides fast error decay.

To make update of projection matrices in each n -th time step, firstly, we need to solve the coarse grid system using only offline multiscale basis functions to find local residuals:

$$S_{T,c}^n \frac{T_c^{n+1} - T_c^n}{\tau} + A_{T,c}^n T_c^{n+1} = G_{T,c},$$

$$A_{p,c}^n p_c^{n+1} = G_{p,c},$$
(22)

where

$$\begin{aligned} S_{T,c}^n &= R_T^n S_T^n (R_T^n)^T, \quad A_{T,c}^n = R_T^n A_T^n (R_T^n)^T, \quad G_{T,c} = R_T^n G_T, \quad T_{ms}^{n+1} = (R_T^n)^T T_c^{n+1}, \\ A_{p,c}^n &= R_p^n A_p^n (R_p^n)^T, \quad G_{p,c} = R_p^n G_p, \quad p_{ms}^{n+1} = (R_p^n)^T p_c^{n+1}, \end{aligned}$$

where T_{ms}^{n+1} , p_{ms}^{n+1} are multiscale solutions that reconstructed on fine grid, R_T^n and R_p^n are predefined projection matrices without enrichment with online bases at n -th time layer

$$\begin{aligned} R_T^n &= R_T = (\psi_{T,1}^1, \dots, \psi_{T,N_c}^1, \dots, \psi_{T,1}^{N_c}, \dots, \psi_{T,N_c}^{N_c}, \psi_{add}^1, \dots, \psi_{add}^{N_p})^T, \\ R_p^n &= R_p = (\psi_{p,1}^1, \dots, \psi_{p,M_{N_c}}^1, \dots, \psi_{p,1}^{N_c}, \dots, \psi_{p,M_{N_c}}^{N_c})^T. \end{aligned}$$

To complete online stage with solving coarse system with updating online multiscale bases functions, firstly, we solve the coarse scale system (22) using offline projection matrices R_T^n and R_p^n . Then we add online bases in these matrices and obtain new projection matrices $R_T^{(L,n)}$, $R_p^{(L,n)}$. We use these matrices until the next update procedure, we update projection matrices on each certain n -th time layer. The process can be iterable to add more multiscale online basis functions:

$$\begin{aligned} R_T^n &= R_T^{L,n} = (\psi_{T,1}^1, \dots, \psi_{T,N_c}^1, \dots, \psi_{T,1}^{N_c}, \dots, \psi_{T,N_c}^{N_c}, \psi_{add}^1, \dots, \psi_{add}^{N_p}, \vartheta_{T,l}^1, \dots, \vartheta_{T,l}^{N_c}, \dots, \vartheta_{T,L}^1, \dots, \vartheta_{T,L}^{N_c})^T, \\ R_p^n &= R_p^{L,n} = (\psi_{p,1}^1, \dots, \psi_{p,M_{N_c}}^1, \dots, \psi_{p,1}^{N_c}, \dots, \psi_{p,M_{N_c}}^{N_c}, \vartheta_{p,l}^1, \dots, \vartheta_{p,l}^{N_c}, \dots, \vartheta_{p,L}^1, \dots, \vartheta_{p,L}^{N_c})^T, \end{aligned}$$

where L denotes the number of online iterations. On the time layer where we don't update online bases, we use R_T^n , R_p^n with old online bases.

Next we present a construction of online multiscale basis functions that based on solution of the following problem in each local domain ω_i :

$$\begin{aligned} a_{T,\omega_i}(\Phi_{T,l}^i, v) &= r_{T,\omega_i}^l(v), \\ a_{p,\omega_i}(\Phi_{p,l}^i, w) &= r_{p,\omega_i}^l(w), \end{aligned} \quad l = 1, \dots, L, \quad (23)$$

where

$$\begin{aligned} a_{T,\omega_i}(\Phi_{T,l}^i, v) &= \int_{\Omega} \left(\alpha(\phi_{\Delta}^n) + \rho^+ L \frac{d\phi_{\Delta}}{dT}(T_{ms}^n) \right) \left(\frac{\Phi_{T,l}^i}{\tau} + (\lambda_{\varepsilon}^n \nabla p_{ms}^n \nabla T_{ms}^n) \right) v dx + \\ &\quad + \int_{\Omega} (k(\phi_{\Delta}^n) \nabla \Phi_{T,l}^i, \nabla v) dx, \\ r_{T,\omega_i}^l(v) &= \int_{\Omega} Q v dx - \int_{\Omega} \left(\alpha(\phi_{\Delta}^n) + \rho^+ L \frac{d\phi_{\Delta}}{dT}(T_{ms}^n) \right) \left(\frac{T_{ms}^{n+1} - T_{ms}^n}{\tau} + (\lambda_{\varepsilon}^n \nabla p_{ms}^n \nabla T_{ms}^n) \right) v dx - \\ &\quad - \int_{\Omega} (k(\phi_{\Delta}^n) \nabla T_{ms}^{n+1}, \nabla v) dx, \\ a_{p,\omega_i}(\Phi_{p,l}^i, w) &= \int_{\Omega} (\lambda_{\varepsilon}^n \nabla \Phi_{p,l}^i, \nabla w) dx, \\ r_{p,\omega_i}^l &= \int_{\Omega} F w dx - \int_{\Omega} (\lambda_{\varepsilon}^n \nabla p_{ms}^{n+1}, \nabla w) dx, \end{aligned}$$

with the boundary condition $\Phi_{T,l}^i = 0$, $\Phi_{p,l}^i = 0$ on $\partial\omega_i$. After solving problem (23) we multiply the solution on partition of unity functions to obtain an online multiscale basis functions:

$$\vartheta_{T,l}^i = \Phi_{T,l}^i \chi^i, \quad \vartheta_{p,l}^i = \Phi_{p,l}^i \chi^i. \quad (24)$$

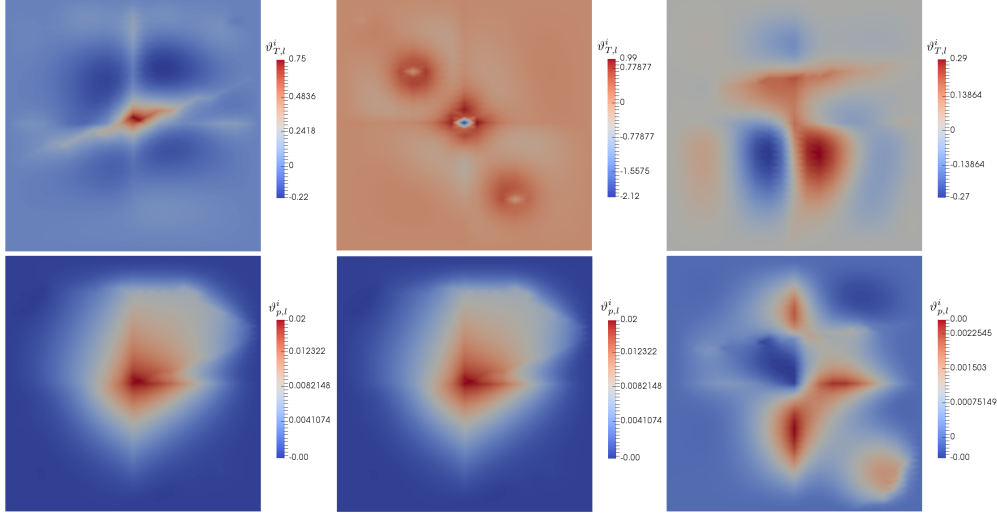


Figure 3: An example of online multiscale basis functions in three local domains ω_i . First row: bases for temperature. Second row: bases for pressure.

We demonstrate an example of online multiscale basis functions in Figure 3.

Next we update multiscale spaces with online basis functions:

$$\begin{aligned} V_{ms}^T &= \text{span}\{\psi_{T,1}^1, \dots, \psi_{T,N_c}^1, \dots, \psi_{T,1}^{N_c}, \dots, \psi_{T,N_c}^{N_c}, \psi_{add}^1, \dots, \psi_{add}^{N_p}, \vartheta_{T,l}^1, \dots, \vartheta_{T,l}^{N_c}\}, \\ V_{ms}^P &= \text{span}\{\psi_{p,1}^1, \dots, \psi_{p,M_{N_c}}^1, \dots, \psi_{p,1}^{N_c}, \dots, \psi_{p,M_{N_c}}^{N_c}, \vartheta_{p,l}^1, \dots, \vartheta_{p,l}^{N_c}\}, \end{aligned} \quad l = 1, \dots, L.$$

Next, we use current solutions $T_{ms}^{l,n}$, $p_{ms}^{l,n}$ to find a certain number of online basis functions in each local domain ω_i :

$$\begin{aligned} S_{T,c}^{l,n} \frac{T_c^{l,n+1} - T_c^{l,n}}{\tau} + A_{T,c}^{l,n} T_c^{l,n+1} &= G_{T,c}, \\ A_{p,c}^{l,n} p_c^{l,n+1} &= G_{p,c}, \end{aligned} \quad (25)$$

where

$$\begin{aligned} S_{T,c}^{l,n} &= R_T^{l,n} S_T^{l,n} (R_T^{l,n})^T, \quad A_{T,c}^{l,n} = R_T^{l,n} A_T^{l,n} (R_T^{l,n})^T, \quad G_{T,c} = R_T^{l,n} G_T, \quad T_{ms}^{l,n+1} = (R_T^{l,n})^T T_c^{l,n+1}, \\ A_{p,c}^{l,n} &= R_p^{l,n} A_p^{l,n} (R_p^{l,n})^T, \quad G_{p,c} = R_p^{l,n} G_p, \quad p_{ms}^{l,n+1} = (R_p^{l,n})^T p_c^{l,n+1}, \end{aligned}$$

and

$$\begin{aligned} R_T^{l,n} &= (\psi_{T,1}^1, \dots, \psi_{T,N_c}^1, \dots, \psi_{T,1}^{N_c}, \dots, \psi_{T,N_c}^{N_c}, \psi_{add}^1, \dots, \psi_{add}^{N_p}, \vartheta_{T,l}^1, \dots, \vartheta_{T,l}^{N_c})^T, \\ R_p^{l,n} &= R_p^{L,n} = (\psi_{p,1}^1, \dots, \psi_{p,M_{N_c}}^1, \dots, \psi_{p,1}^{N_c}, \dots, \psi_{p,M_{N_c}}^{N_c}, \vartheta_{p,l}^1, \dots, \vartheta_{p,l}^{N_c})^T, \end{aligned}$$

with $l = 1, \dots, L$, $R_T^n = R_T^{L,n}$, $R_p^n = R_p^{L,n}$.

5 Numerical results

In this paper, we consider problems in two-dimensional formulation in heterogeneous domain with high contrast. We consider modeling of heat and mass transfer in computational domain $\Omega = [12 \times 6][m]$. For modeling, we take 20 freezing pipes in computational domain. Our heterogeneity is represented by layers and simulates a layered reservoir. We construct structured triangular fine grid $[120 \times 120]$ with 14641 vertices and 14400 cells. For multiscale solver, we generate coarse grid 24×12 with 325 vertices and 288 cells. Computational domain, computational grid and schematic heterogeneity are presented in fig. 4.

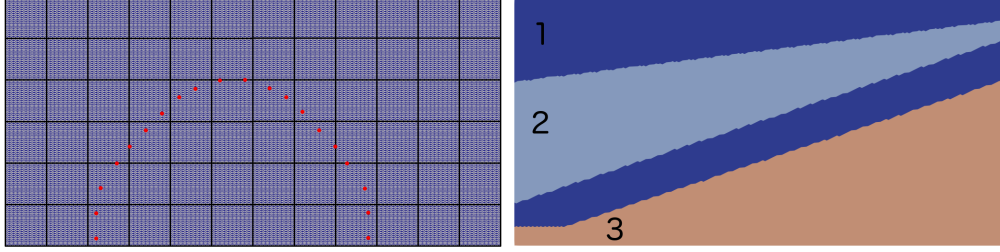


Figure 4: The computational grid with 20 freezing pipes and heterogeneity. Left: coarse grid and fine grid. Right: heterogeneous properties.

We perform modeling of ground freezing process with $t_{max} = 25$ days and 80 times steps. In our simulation we set Dirichlet boundary condition on the freezing pipes $T_p = -30^\circ C$ and on the other boundaries we set $-k \frac{\partial T}{\partial n} = 0$. As initial condition for temperature we take $T_0 = 2^\circ C$. For pressure we take different boundary conditions:

- *Test 1.* Flow from right to left, at the left boundary we set $p = 1$, on the right boundary $-p = 0$,
- *Test 2.* Flow from right to left, at the top boundary we set $p = 1$, on the bottom boundary $-p = 0$.

On the other boundaries for pressure, we apply $-\lambda_\varepsilon \frac{\partial p}{\partial n} = 0$.

We take the next values of coefficients:

$$\begin{aligned}
 \lambda_1^+ &= 1.37[W/(m \cdot K)], \quad \lambda_1^- = 1.72[W/(m \cdot K)], \quad c_1^+ \rho_1^+ = 2.397 \cdot 10^6[J/(m^3 \cdot K)], \\
 c_1^- \rho_1^- &= 1.886 \cdot 10^6[J/(m^3 \cdot K)], \quad \rho_1^+ L_1 = 75.33 \cdot 10^6, \quad \frac{\rho_{w,1} \kappa_1}{\mu_1} = 1.0 \cdot 10^{-13}, \\
 \lambda_2^+ &= 2.67[W/(m \cdot K)], \quad \lambda_2^- = 3.37[W/(m \cdot K)], \quad c_2^+ \rho_2^+ = 2.13 \cdot 10^6[J/(m^3 \cdot K)], \\
 c_2^- \rho_2^- &= 2.09 \cdot 10^6[J/(m^3 \cdot K)], \quad \rho_2^+ L_2 = 64.769 \cdot 10^6, \quad \frac{\rho_{w,2} \kappa_2}{\mu_2} = 10.0 \cdot 10^{-13}, \\
 \lambda_3^+ &= 1.4[W/(m \cdot K)], \quad \lambda_3^- = 1.56[W/(m \cdot K)], \quad c_3^+ \rho_3^+ = 2.96 \cdot 10^6[J/(m^3 \cdot K)], \\
 c_3^- \rho_3^- &= 2.70 \cdot 10^6[J/(m^3 \cdot K)], \quad \rho_2^+ L_2 = 130.544 \cdot 10^6, \quad \frac{\rho_{w,2} \kappa_2}{\mu_2} = 5.0 \cdot 10^{-13}, \\
 \varepsilon &= 10^{-3}, \quad \Delta = 0.5, \quad Q = 0, \quad F = 0.
 \end{aligned}$$

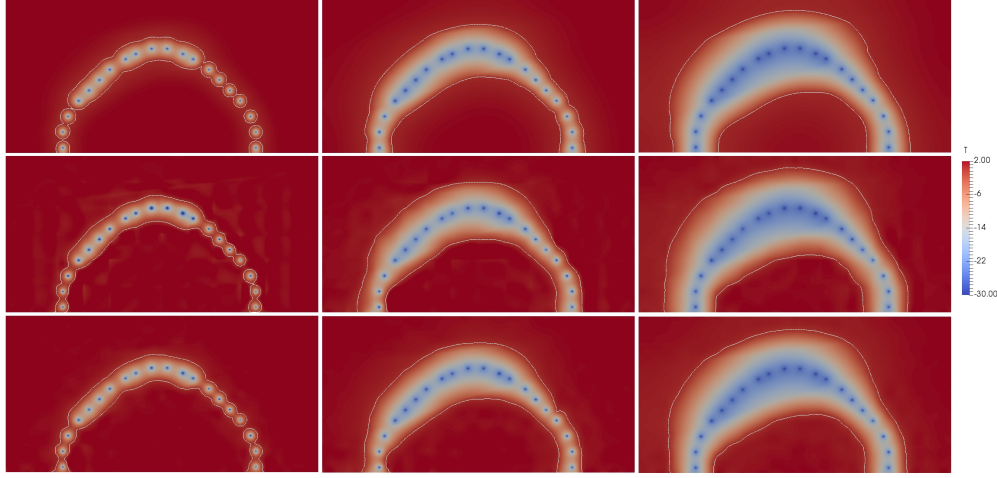


Figure 5: Distribution of Temperature for *Test 1* on 5, 30 and 80 time layers. First row: fine grid solution. Second row: multiscale solution using 4 offline basis functions. Third row: multiscale solution using 4 offline basis functions and 1 online basis function.

We will examine the multiscale and fine grid solutions for numerical results validation. To do this, we use relative errors in L_2 and H_1 norms:

$$\|e\|_{L_2} = \sqrt{\frac{\int_{\Omega} (u_f - u_{ms})^2 dx}{\int_{\Omega} u_f^2 dx}}, \quad \|e\|_{H_1} = \sqrt{\frac{\int_{\Omega} (\nabla(u_f - u_{ms}), \nabla(u_f - u_{ms})) dx}{\int_{\Omega} (\nabla u_f, \nabla u_f) dx}}, \quad (26)$$

where u_f is a solution on a fine grid obtained by finite element method, u_{ms} is a multiscale solution, instead of function u we use temperature T and pressure p .

Number of offline basis functions	Offline basis			1 Online basis			2 Online basis		
	DOF_c	$e_T^{L_2}$	$e_T^{H_1}$	DOF_c	$e_T^{L_2}$	$e_T^{H_1}$	DOF_c	$e_T^{L_2}$	$e_T^{H_1}$
2	397	11.701	31.393	579	6.111	18.639	761	4.728	11.606
4	761	8.222	21.188	943	5.484	13.826	1125	4.221	11.266
6	1125	7.159	18.023	1307	4.893	12.438	1489	3.537	10.031
8	1489	5.356	15.113	1671	3.757	10.174	1853	3.386	9.529

Table 1: Numerical results for *Test 1*. Relative L_2 and H_1 (%) errors for Temperature with different number of offline multiscale basis functions using 1 and 2 online basis functions on the last time layer.

On several time layers, we display a temperature distribution *Test 1* in Figure 5, pressure distribution in time are shown in Figure 5. In these figures in first row we present a fine grid solution, in second row we present a multiscale solution using 4 offline multiscale basis functions in each local domain and in third row we present a multiscale solution with 4 offline and 1 online multiscale basis functions. The additional basis

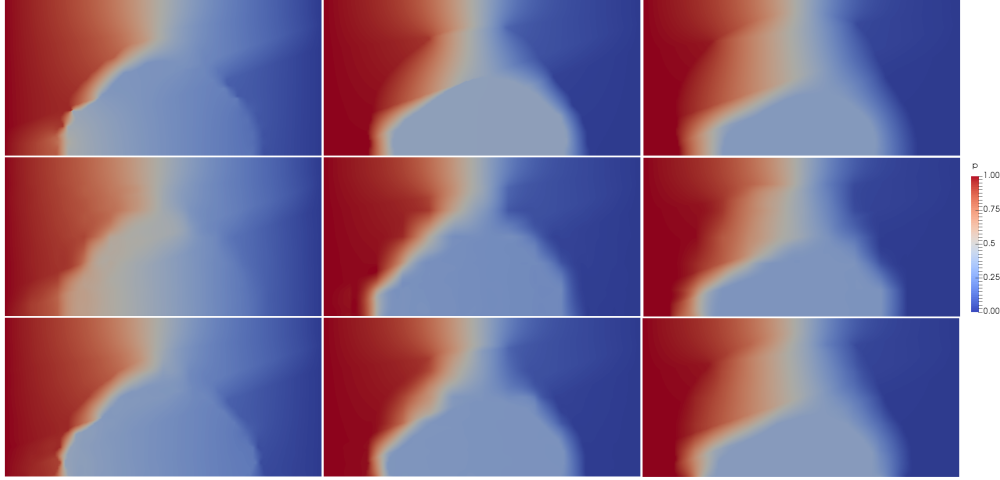


Figure 6: Distribution of Pressure for *Test 1* on 5, 30 and 80 time layers. First row: fine grid solution. Second row: multiscale solution using 4 offline basis functions. Third row: multiscale solution using 4 offline basis functions and 1 online basis function.

Number of offline basis functions	Offline basis			1 Online basis			2 Online basis		
	DOF_c	$e_p^{L_2}$	$e_p^{H_1}$	DOF_c	$e_p^{L_2}$	$e_p^{H_1}$	DOF_c	$e_p^{L_2}$	$e_p^{H_1}$
2	397	15.817	66.365	579	1.831	28.653	761	1.149	21.409
4	761	5.826	48.115	943	1.881	26.970	1125	1.556	24.346
6	1125	4.603	44.995	1307	1.913	25.779	1489	1.519	22.885
8	1489	3.799	40.171	1671	1.431	21.668	1853	1.221	19.637

Table 2: Numerical results for *Test 1*. Relative L_2 and H_1 (%) errors for Pressure with different number of offline multiscale basis functions using 1 and 2 online basis functions on the last time layer.

functions (2) is used in each computation in the set of offline basis functions. In Figure 5 the phase change boundary is drawn by a white line. One can see that our method describes the phase change boundary with high accuracy. We should note, that we enrich multiscale space by online basis function on each 5-th time layer.

We show the relative L_2 and H_1 errors for temperature in Table 1 and for pressure in Table 2. In these tables, we show the comparison between simple GMsFEM and Online GMsFEM, using 1 and 2 online basis functions. From the tables, one can see, that we have a big error decay when we are using online basis functions. The proposed method has almost no difference in accuracy between using 1 and 2 online basis functions. We denote by DOF_c a number of degree of freedom on the coarse grid. In Figures 11 and 8 we present L_2 and H_1 errors distribution in time for temperature and pressure respectively. The graphics present the errors for 4 offline multiscale basis functions with 0,1 or 2 online basis functions. For online

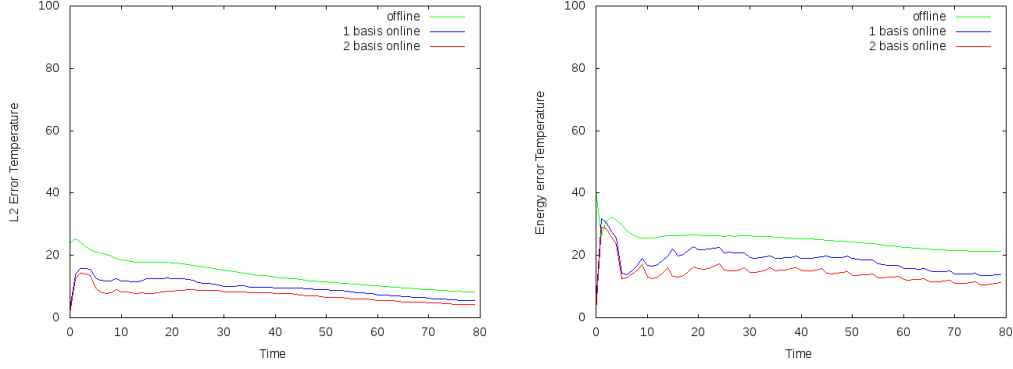


Figure 7: Numerical results for *Test 1*. Error comparison for Temperature between offline approach using 4 offline basis and online approach using 1 and 2 online basis. Left: L_2 error. Right: H_1 error.

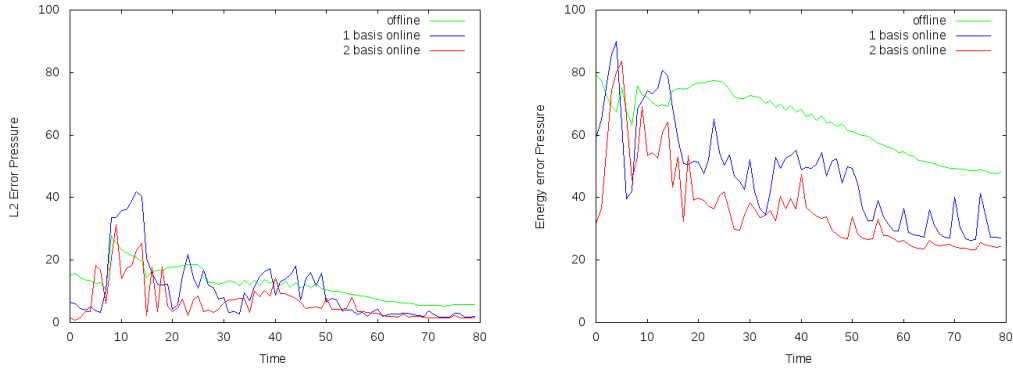


Figure 8: Numerical results for *Test 1*. Error comparison for Pressure between offline approach using 4 offline basis and online approach using 1 and 2 online basis. Left: L_2 error. Right: H_1 error.

GMsFEM, we can observe the errors fall on each 5-th time layer. The error jumps are smaller when we use 2 online multiscale basis functions. From that, we can conclude that is better to use 2 online basis functions in each ω_i .

For *Test 2* we present numerical results in Figure 9 for temperature and in Figure 10 for pressure. The multiscale solution is obtained by using 4 offline basis functions and additional basis. The fine grid solution is presented in the first row of the Figures, the offline solution is presented in the second row and in the third row we show the solution using 1 online multiscale basis functions. We can observe the good approximation of phase change boundary by Online GMsFEM. The change of flow direction in pressure didn't seem to affect the accuracy of the method. More accurate conclusions can be drawn by looking at the errors.

The relative L_2 and H_1 errors for *Test 2* are presented in Tables 3 and 4. The errors are shown for offline solution using 4 offline basis functions and for solutions with 1 and 2 online basis functions. The behavior of the errors is the same from *Test 1*. But here we have a little difference in behavior using online bases. Here

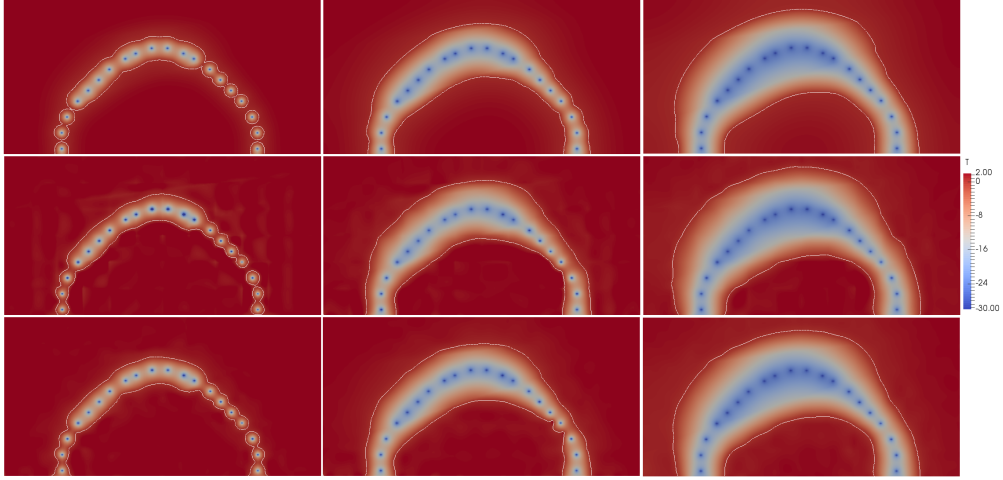


Figure 9: Distribution of Temperature for *Test 2* on 5, 30 and 80 time layers. First row: fine grid solution. Second row: multiscale solution using 4 offline basis functions. Third row: multiscale solution using 4 offline basis functions and 1 online basis function.

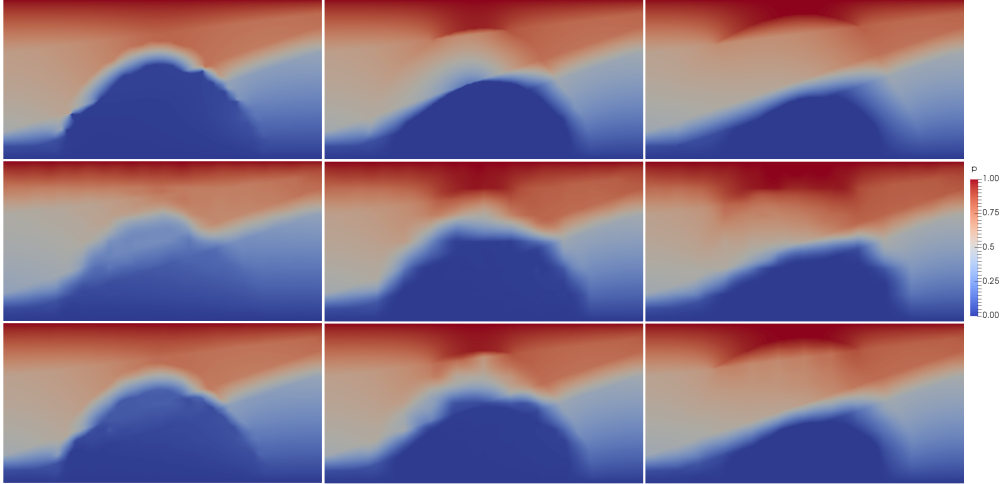


Figure 10: Distribution of Pressure for *Test 2* on 5, 30 and 80 time layers. First row: fine grid solution. Second row: multiscale solution using 4 offline basis functions. Third row: multiscale solution using 4 offline basis functions and 1 online basis function.

we have a bigger difference in temperature error between the results with 1 and 2 online basis functions. One can see the error falling with adding second online basis more clearly. As in *Test1*, the online approach allows taking less number of offline multiscale basis functions. We also demonstrate the error distribution in time with 4 offline basis functions using 1 and 2 online bases in Figure 11 for temperature and for pressure in Figure 12. We also can see the error decay on each 5-th time layer. The jump of the error is smaller when

Number of offline basis functions	Offline basis			1 Online basis			2 Online basis		
	DOF_c	$e_T^{L_2}$	$e_T^{H_1}$	DOF_c	$e_T^{L_2}$	$e_T^{H_1}$	DOF_c	$e_T^{L_2}$	$e_T^{H_1}$
2	397	13.631	35.347	579	10.064	25.264	761	4.434	10.333
4	761	7.709	20.231	943	4.129	11.337	1125	2.919	8.693
6	1125	6.462	16.861	1307	3.819	10.510	1489	2.663	8.028
8	1489	5.103	14.521	1671	3.021	8.857	1853	2.539	7.475

Table 3: Numerical results for *Test 2*. Relative L_2 and H_1 (%) errors for Pressure with different number of offline multiscale basis functions using 1 and 2 online basis functions on the last time layer.

we use 2 online basis functions. In this case, the adding of second online basis functions is also justified.

Number of offline basis functions	Offline basis			1 Online basis			2 Online basis		
	DOF_c	$e_p^{L_2}$	$e_p^{H_1}$	DOF_c	$e_p^{L_2}$	$e_p^{H_1}$	DOF_c	$e_p^{L_2}$	$e_p^{H_1}$
2	397	13.009	58.768	579	4.786	25.264	761	2.741	20.211
4	761	8.341	48.899	943	2.491	20.659	1125	1.524	17.468
6	1125	7.292	46.295	1307	1.801	17.433	1489	1.124	13.675
8	1489	5.811	41.757	1671	1.371	14.712	1853	1.071	12.517

Table 4: Numerical results for *Test 2*. Relative L_2 and H_1 (%) errors for Pressure with different number of offline multiscale basis functions using 1 and 2 online basis functions on the last time layer.

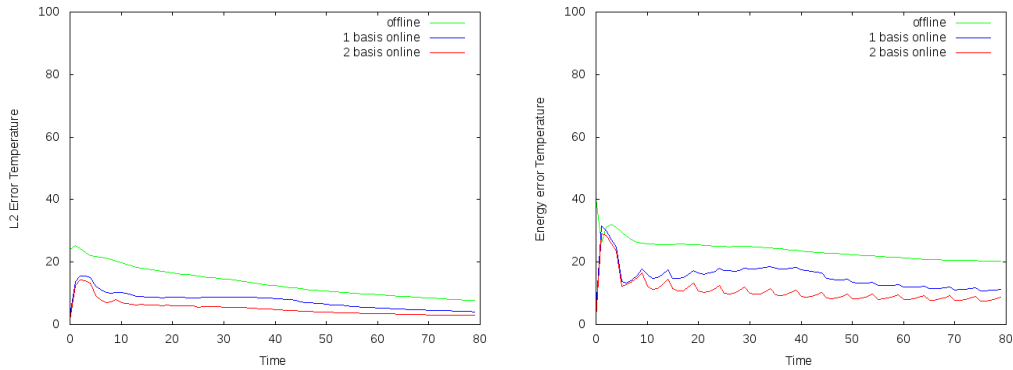


Figure 11: Numerical results for *Test 2*. Error comparison for Temperature between offline approach using 4 offline basis and online approach using 1 and 2 online basis. Left: L_2 error. Right: H_1 error.

We need to discuss obtained results. The Online GMsFEM showed a good results in both cases. We should note that we did not show the results without an additional basis functions due to the fact that

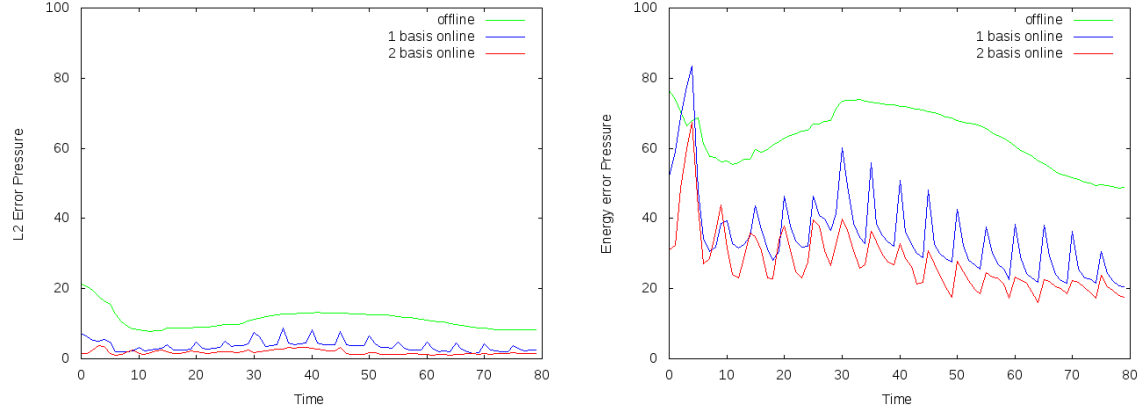


Figure 12: Numerical results for *Test 2*. Error comparison for Pressure between offline approach using 4 offline basis and online approach using 1 and 2 online basis. Left: L_2 error. Right: H_1 error.

these results were obtained by us in our previous work [46], which shows the effectiveness of the additional bases. We need to decide about the number of online basis functions. And we need to mention In the *Test 1* we have a little error fall with adding second online basis, but in *Test 2* we have a bigger error falling for temperature. But in both cases the second online basis reduced the error jump in time. So, the question of adding a second basis is for the desired purposes. If for a certain study we want to know only the final state, then just enough only 1 online basis. If we need to know the solution at every moment of time, then we should use 2 online bases.

6 Conclusion

An online generalized multiscale finite element method for heat and mass problem in heterogeneous media with artificial ground freezing was proposed in this study. We considered two test cases with different boundary condition for pressure. We did a numerical experiment to demonstrate the method's correctness. We demonstrated multiscale solutions with various numbers of offline and online multiscale basis functions during the experiment. The experiment clearly showed that the addition of online basis function greatly improves the accuracy of GMsFEM. But whether to add a second online basis function already depends on the goals of the study. Nevertheless, in all the performed experiments, we obtained good error rates. We have significant decrease of the original system while not losing in terms of accuracy. An online generalized multiscale finite element method can be used for modeling heat and mass transfer problems.

7 Acknowledgements

This work is supported the grant of Russian Science Foundation N21-71-00061 and the Russian government project Science and Universities (project FSRG-2021-0015) aimed at supporting junior laboratories.

References

- [1] Orlando B Andersland and Branko Ladanyi. *Frozen ground engineering*. John Wiley & Sons, 2003.
- [2] John S Harris. *Ground freezing in practice*. Thomas Telford, 1995.
- [3] Greg Newman, Lori Newman, Denise Chapman, and Travis Harbicht. Artificial ground freezing: An environmental best practice at cameco’s uranium mining operations in northern saskatchewan, canada. *Rüde, Freund# Wolkersdorfer (Editors)*, pages 113–118, 2011.
- [4] Mahmoud A Alzoubi, Agus P Sasmito, Ali Madiseh, and Ferri P Hassani. Intermittent freezing concept for energy saving in artificial ground freezing systems. *Energy Procedia*, 142:3920–3925, 2017.
- [5] Hans L Jessberger. Theory and application of ground freezing in civil engineering. *Cold Regions Science and Technology*, 3(1):3–27, 1980.
- [6] FA Loveridge, A Amis, and William Powrie. Energy pile performance and preventing ground freezing. 2012.
- [7] Wenping Fei, Zhaohui Joey Yang, and Tiecheng Sun. Ground freezing impact on laterally loaded pile foundations considering strain rate effect. *Cold Regions Science and Technology*, 157:53–63, 2019.
- [8] M Vasilyeva, S Stepanov, and I Sirditov. Reduced dimension model for heat transfer of ground heat exchanger in permafrost. In *Journal of Physics: Conference Series*, volume 937, page 012056. IOP Publishing, 2017.
- [9] David C Esch. Thermal analysis, construction, and monitoring methods for frozen ground. American Society of Civil Engineers, 2004.
- [10] Vasilios Alexiades and Alan D Solomon. *Mathematical modeling of melting and freezing processes*. Routledge, 2018.
- [11] Klaus-Jürgen Bathe. Finite element method. *Wiley encyclopedia of computer science and engineering*, pages 1–12, 2007.
- [12] Barna Szabó and Ivo Babuška. Finite element analysis: Method, verification and validation. 2021.
- [13] NG Burago and AI Fedyushkin. Numerical solution of the stefan problem. In *Journal of Physics: Conference Series*, volume 1809, page 012002. IOP Publishing, 2021.
- [14] Rubinshteĭ. *The stefan problem*.
- [15] Roland Glowinski, Tsorng-Whay Pan, and Jacques Periaux. A fictitious domain method for dirichlet problem and applications. *Computer Methods in Applied Mechanics and Engineering*, 111(3-4):283–303, 1994.

- [16] Roland Glowinski, Tsorng-Whay Pan, and Jacques Periaux. A fictitious domain method for external incompressible viscous flow modeled by navier-stokes equations. *Computer Methods in Applied Mechanics and Engineering*, 112(1-4):133–148, 1994.
- [17] Alexey Talonov and Maria Vasilyeva. On numerical homogenization of shale gas transport. *Journal of Computational and Applied Mathematics*, 301:44–52, 2016.
- [18] Vasiliy Grigoriev, Petr Zakharov, and Mir Akimov. Effective calculation of thermophysical properties of composite materials with multiple configurations by asymptotic homogenization technique. In *Journal of Physics: Conference Series*, volume 1392, page 012069. IOP Publishing, 2019.
- [19] U Gavrilieva, V Alekseev, and M Vasilyeva. Numerical homogenization for wave propagation in fractured media. In *AIP Conference Proceedings*, volume 2025, page 100002. AIP Publishing LLC, 2018.
- [20] Yalchin Efendiev and Thomas Y Hou. *Multiscale finite element methods: theory and applications*, volume 4. Springer Science & Business Media, 2009.
- [21] Thomas Y Hou and Xiao-Hui Wu. A multiscale finite element method for elliptic problems in composite materials and porous media. *Journal of computational physics*, 134(1):169–189, 1997.
- [22] I Yucel Akkutlu, Yalchin Efendiev, Maria Vasilyeva, and Yuhe Wang. Multiscale model reduction for shale gas transport in a coupled discrete fracture and dual-continuum porous media. *Journal of Natural Gas Science and Engineering*, 2017.
- [23] Hadi Hajibeygi, Giuseppe Bonfigli, Marc Andre Hesse, and Patrick Jenny. Iterative multiscale finite-volume method. *Journal of Computational Physics*, 227(19):8604–8621, 2008.
- [24] Ivan Lunati and Patrick Jenny. Multiscale finite-volume method for compressible multiphase flow in porous media. *Journal of Computational Physics*, 216(2):616–636, 2006.
- [25] Ivan Lunati and Patrick Jenny. Multiscale finite-volume method for density-driven flow in porous media. *Computational Geosciences*, 12(3):337–350, 2008.
- [26] Aleksei Tyrylgina, Maria Vasilyeva, and Eric T Chung. Embedded fracture model in numerical simulation of the fluid flow and geo-mechanics using generalized multiscale finite element method. In *Journal of Physics: Conference Series*, volume 1392, page 012075. IOP Publishing, 2019.
- [27] Robert Eymard, Thierry Gallouët, and Raphaële Herbin. Finite volume methods. *Handbook of numerical analysis*, 7:713–1018, 2000.
- [28] Fadl Moukalled, Luca Mangani, and Marwan Darwish. The finite volume method. In *The finite volume method in computational fluid dynamics*, pages 103–135. Springer, 2016.
- [29] Eric Chung, Yalchin Efendiev, and Thomas Y Hou. Adaptive multiscale model reduction with generalized multiscale finite element methods. *Journal of Computational Physics*, 320:69–95, 2016.

- [30] Eric T Chung, Yalchin Efendiev, and Shubin Fu. Generalized multiscale finite element method for elasticity equations. *GEM-International Journal on Geomathematics*, 5(2):225–254, 2014.
- [31] Yalchin Efendiev, Juan Galvis, and Thomas Y Hou. Generalized multiscale finite element methods (gmsfem). *Journal of Computational Physics*, 251:116–135, 2013.
- [32] Eric T Chung, Yalchin Efendiev, and Wing Tat Leung. Constraint energy minimizing generalized multiscale finite element method. *Computer Methods in Applied Mechanics and Engineering*, 339:298–319, 2018.
- [33] Siu Wun Cheung, Eric T Chung, Yalchin Efendiev, Wing Tat Leung, and Maria Vasilyeva. Constraint energy minimizing generalized multiscale finite element method for dual continuum model. *arXiv preprint arXiv:1807.10955*, 2018.
- [34] Shubin Fu, Eric Chung, and Tina Mai. Constraint energy minimizing generalized multiscale finite element method for nonlinear poroelasticity and elasticity. *Journal of Computational Physics*, 417:109569, 2020.
- [35] Zhiming Chen and Thomas Hou. A mixed multiscale finite element method for elliptic problems with oscillating coefficients. *Mathematics of Computation*, 72(242):541–576, 2003.
- [36] Eric T Chung, Yalchin Efendiev, and Chak Shing Lee. Mixed generalized multiscale finite element methods and applications. *Multiscale Modeling & Simulation*, 13(1):338–366, 2015.
- [37] Jørg E Aarnes, Yalchin Efendiev, and Lijian Jiang. Mixed multiscale finite element methods using limited global information. *Multiscale Modeling & Simulation*, 7(2):655–676, 2008.
- [38] Ibrahim Y Akkutlu, Yalchin Efendiev, and Maria Vasilyeva. Multiscale model reduction for shale gas transport in fractured media. *Computational Geosciences*, 20(5):953–973, 2016.
- [39] Eric T Chung, Yalchin Efendiev, and Wing Tat Leung. Residual-driven online generalized multiscale finite element methods. *Journal of Computational Physics*, 302:176–190, 2015.
- [40] Aleksei Tyrylgina, Yaoyao Chen, Maria Vasilyeva, and Eric T Chung. Multiscale model reduction for the allen–cahn problem in perforated domains. *Journal of Computational and Applied Mathematics*, 381:113010, 2021.
- [41] Denis Spiridonov, Maria Vasilyeva, Aleksei Tyrylgina, and Eric T Chung. An online generalized multiscale finite element method for unsaturated filtration problem in fractured media. *Mathematics*, 9(12):1382, 2021.
- [42] Eric T Chung, Yalchin Efendiev, Wing Tat Leung, Maria Vasilyeva, and Yating Wang. Non-local multi-continua upscaling for flows in heterogeneous fractured media. *Journal of Computational Physics*, 2018.

- [43] Maria Vasilyeva, Eric T Chung, Siu Wun Cheung, Yating Wang, and Georgy Prokopev. Nonlocal multi-continua upscaling for multicontinua flow problems in fractured porous media. *Journal of Computational and Applied Mathematics*, 2019.
- [44] Maria Vasilyeva, Eric T Chung, Yalchin Efendiev, and Jihoon Kim. Constrained energy minimization based upscaling for coupled flow and mechanics. *Journal of Computational Physics*, 376:660–674, 2019.
- [45] Maria Vasilyeva, Eric T Chung, Wing Tat Leung, Yating Wang, and Denis Spiridonov. Upscaling method for problems in perforated domains with non-homogeneous boundary conditions on perforations using non-local multi-continuum method (nlmc). *Journal of Computational and Applied Mathematics*, 357:215–227, 2019.
- [46] Maria Vasilyeva, Sergei Stepanov, Denis Spiridonov, and Vasilii Vasil’ev. Multiscale finite element method for heat transfer problem during artificial ground freezing. *Journal of Computational and Applied Mathematics*, 371:112605, 2020.
- [47] A. A. Samarskiy and P. N. Vabishchevich. *Computational heat transfer*. Librocom, 2009.
- [48] L I Rubinstein. *Stefan problem*. Zweigzine, 1967.
- [49] AA Samarskii, PN Vabishchevich, OP Iliev, and AG Churbanov. Numerical simulation of convection/diffusion phase change problems—a review. *International journal of heat and mass transfer*, 36(17):4095–4106, 1993.
- [50] YOUSSEF Belhamadia, ABDOULAYE S Kane, and ANDRÉ Fortin. An enhanced mathematical model for phase change problems with natural convection. *International Journal of Numerical Analysis and Modeling*, 3(2):192–206, 2012.
- [51] Madhuchhanda Bhattacharya, Tanmay Basak, and KG Ayappa. A fixed-grid finite element based enthalpy formulation for generalized phase change problems: role of superficial mushy region. *International Journal of Heat and Mass Transfer*, 45(24):4881–4898, 2002.
- [52] P. N. Vabishchevich, Vasilyeva M. V., and Pavlova N. V. Numerical modeling of thermal stabilization of filter soils [in russian]. *Mathematical modeling*, 26(9):111–125, 2014.
- [53] Vasily Vasil’ev and Maria Vasilyeva. An accurate approximation of the two-phase stefan problem with coefficient smoothing. *Mathematics*, 8(11):1924, 2020.
- [54] Maria Vasilyeva, Sergei Stepanov, Denis Spiridonov, and Vasilii Vasil’ev. Multiscale finite element method for heat transfer problem during artificial ground freezing. *Journal of Computational and Applied Mathematics*, 371:112605, 2020.